Spectrochimica Acta Part A: Molecular and Biomolecular Spectroscopy 227 (2020) 117682

Contents lists available at ScienceDirect

Spectrochimica Acta Part A: Molecular and Biomolecular Spectroscopy

journal homepage: www.elsevier.com/locate/saa

The study of the interaction mechanism between bovine serum albumin and single-walled carbon nanotubes depending on their diameter and concentration in solid nanocomposites by vibrational spectroscopy

Alexander Yu. Gerasimenko [a, d, *], Galina N. Ten [b], Dmitry I. Ryabkin [a], Natalia E. Shcherbakova [c], Elena A. Morozova [d], Levan P. Ichkitidze [a, d]

[a] National Research University of Electronic Technology MIET, Shokin Square, Zelenograd, Moscow, 124498, Russia
[b] Saratov State University, 83 Astrakhanskaya street, Saratov, 410012, Russia
[c] Russian Research Anti-Plague Institute "Microbe", 46 Universitetskaya street, Saratov, 410005, Russia
[d] I.M. Sechenov First Moscow State Medical University, bld. 2-4, Bolshaya Pirogovskaya street, Moscow, 119991, Russia

ARTICLE INFO

Article history:
Received 6 June 2019
Received in revised form
16 October 2019
Accepted 19 October 2019
Available online 23 October 2019

Keywords:
Bovine serum albumin (BSA)
Single-walled carbon nanotubes (SWCNT)
Amino acid
Nanocomposite
Covalent and hydrophobic interactions
Cells viability
FTIR and Raman spectroscopy

ABSTRACT

The results of the study of composites based on bovine serum albumin (BSA) and single-walled carbon nanotubes (SWCNT) are presented. Nanocomposites were created by evaporation of the water-albumin dispersion with nanotubes using diode laser with temperature control. Two types of nanotubes were used. SWCNT I were synthesized using the electric arc method, SWCNT II were synthesized using the gas phase method. SWCNT I had a diameter and length less than SWCNT II. The mechanism of interaction between BSA and SWCNT in solid nanocomposites is considered. An experimental and theoretical studies of the interaction between aspartic (Asp) and glutamic (Glu) amino acids located on the outer surface of BSA and nanotubes using of vibrational spectroscopy (Fourier-transform infrared (FTIR) and Raman spectroscopy) was carried out. The possibility of nanotubes functionalization by oxygen atoms of negative amino acid residues Asp and Glu, which are on the outer surface of BSA, is shown by molecular modeling. The formation of covalent bonds between BSA and SWCNT in nanocomposites with different concentrations of nanotubes (0.01, 0.1 and 1 g/l) was confirmed by vibrational spectra. The covalent interaction between BSA with SWCNT under the laser irradiation leads to the conformational changes in the secondary and tertiary structures of albumin. This is confirmed by a significant decrease in the intensity of the absorption bands in the high-frequency region. The calculation of the vibrational spectra of the three Glycine:Glycine, Glutamic acid:Threonine and Aspartic acid:Lysine complexes, which take into account hydrogen, ion-dipole and ion-ion bonds, showed that a disturbance in the intermolecular interaction between amino acid residues led to significant decrease in the intensity of absorption bands in the region of stretching vibrations bonds OH and NH. From the Raman spectra, it was found that a significant number of defects in SWCNT is caused by the covalent attachment of oxygen atoms to the graphene surface of nanotubes. An increase in the diameter of nanotubes (4 nm) has practically no effect on the absorption spectrum of nanocomposite, while measuring the concentration of SWCNT affects the FTIR spectra. This confirmed the hydrophobic interaction between BSA and SWCNT. Thus, it was shown that BSA solid nanocomposites with CNTs can interact either with the help of hydrophobic forces or with the formation of covalent bonds, which depends on the diameter of the used nanotubes. The viability of connective fibroblast tissue cells on nanocomposites with both types of SWCNT was demonstrated. It was found that nanocomposites based on SWCNT I provide slightly better compatibility of their structure with fibroblasts. It allows to achieve better cell adhesion to the nanocomposite surface. These criteria make extensive use of scaffold nanocomposites in biomedicine, depending on the requirements for their quality and application.

1. Introduction

Nanobiomedicine is currently one of the most actively and successfully developing areas of nanotechnology. Developments in

* Corresponding author. National Research University of Electronic Technology MIET, Shokin Square, Zelenograd, Moscow, 124498, Russia.
E-mail address: gerasimenko@bms.zone (A.Yu. Gerasimenko).

https://doi.org/10.1016/j.saa.2019.117682
1386-1425/

this area allow us to move to a new level of diagnosis and treatment of many diseases. Carbon nanotubes (CNT) are widely used in this area. Due to their unique properties, it becomes possible to create nanomaterials based on CNT. The basic properties (mechanical, electrical, optical, and thermal) of CNT are well studied and can be purposefully changed as a result of various topological modifications of nanotubes. CNT have dimensions close to those of the main components of the natural cellular matrix; their mechanical properties are similar to those of protein structures [1–3].

The creation of new bio-nanomaterials requires a clarification of the nature and details of the interaction between the biological and nano components. Currently, the processes of binding molecules of biopolymers and synthetic carbon nanomaterials for creating implants (especially for cardiac surgery), biosensors, drug carriers and visualization are being actively studied [4–6].

There are a number of works where the non-specific nature of the adsorption of proteins on the surface of nanotube is noted, a brief overview of which is presented in Ref. [7]. This is due to the large variety of protein structures and their properties. The study of the interaction between CNT and the main biological polymers (DNA, poly (A), ribonuclease A, collagen, albumin) using Raman method and electron spectroscopy allowed to conclude about the nature of non-covalent interactions in the nanotube-biomolecule system. As a result of the conformational analysis, the formation of sufficiently stable DNA-nanotube complexes with the van der Waals interaction is observed.

The study of the characteristics of the interaction between CNT and proteins is an urgent task. Bovine serum albumin (BSA) plays the role of a biocompatible dispersant for single-walled carbon nanotubes (SWCNT) [8]. It allows to evenly distribute SWCNT with a concentration of 0.3 g/l over the entire volume of various types of human cells, while retaining the unique properties inherent in SWCNT. In order to improve the dispersion of SWCNT in plasma, it is advisable to functionalize them with carboxyl groups [9]. At the same time, a decrease in BSA fluorescence intensity is observed. This confirms the hydrophobic interaction between amino acid residues and nanotubes. To determine the conformational changes of BSA molecules, the spectrum of circular dichroism was used. It showed a decrease in α-helical albumin structure by 14.06%.

It is known that the insertion of nanotubes into the blood plasma leads to an effective sorption of proteins, including BSA, on the nanotubes surface. Thus, the obtained composite was coated with antibodies. As the result, the immuno-CNT capable to recognize pathogenic *E. coli* were formatted [10].

The interaction between nanotubes and BSA, inside as well as on the nanotube surface, was studied theoretically and experimentally [11,12]. This arrangement of the protein allows to determine the most optimal conditions for using nanotubes for the targeted delivery of drugs and proteins. Three possible model of protein structures (a cylinder, an elongated ellipsoid, three related spheres) were considered to determine the critical size of nanotube that would allow to immobilizate the enzymes through non-covalent and covalent interactions. Knowledge of critical size is crucial in the design of nanomaterials to obtain maximum filling of nanotubes by drugs and protein molecules. Although the covalent interaction provides a long-term attachment of the delivered drug, the structure of the enzyme may be impaired. The conditions under which the creation of stable addition of enzymes is observed, while the activity and function of their native state are maximally preserved [11]. The adhesion of human serum albumin to nanomaterials based on multi-walled carbon nanotubes to create a cardiovascular sensor with the use of Raman spectroscopy was demonstrated [4].

Analysis of the fluorescence and circular dichroism spectra showed that hydrophobic interactions (hydrogen bonds, van der Waals forces, electrostatic forces and hydrophobic interactions) and π-stacking are the main mechanisms that determine the interaction between SWCNT and BSA and their binding in the IB subdomain [13,14]. For the first time, it was shown that the interaction between SWCNT with chirality (5; 5) and proteins leads to the disruption of the secondary and tertiary structure of BSA. Therefore, an adverse effect on the human body may occur upon a contact of nanotubes with proteins [15]. At the same time, the number of experimental works and theoretical calculations that consider the implantation SWCNT into the biological environment is limited, and the interaction processes are not well understood [1,16,17].

The urgent task of modern nanotechnology is the creation of matrix nanocomposites with nanotubes to form tissue-engineering structures for various applications [18–22]. The principal possibility of obtaining nanocomposites by the laser method was shown in Refs. [3,23–25]. The essence of the method lies in the emergence of a nanotube scaffold as a result of the evaporation of the water-albumin dispersion of carbon nanotubes. The formation of C–C bonds occurs in the site of defects of neighboring carbon nanotubes in the scaffold under the laser heating [26,27]. The presence of such scaffold creates the conditions for self-organization of the cellular material of biological tissues, supported by non-covalent bonds in the hydrophobic interaction of tissues. A similar organization of biological macromolecules in nature, for example, is realized in phospholipids, the main components of plasma in cell membranes.

The applied field of research results in this area is the development of cellular and tissue-engineering matrixes for restoring connective (including cartilage) and bone tissue, as well as laser welding of biological tissues with the use of water-protein dispersions of nanoparticles as a solder applied to the welded tissue [28,29]. Earlier, we demonstrated the proliferation of connective tissue cells (fibroblasts) on nanocomposites from BSA and SWCNT, created by pulsed femtosecond laser radiation without a temperature control system [26].

One of the reasons hindering the widespread inculcation of scaffold composite materials in biomedicine, is the lack of clear requirements for the quality of their manufacture. It is obvious that such requirements can be developed if the interaction mechanism between albumin and nanotubes is known.

It was shown earlier that the graphene surface of SWCNT in water solution can interact with BSA only by means of hydrophobic forces. While creating solid scaffold nanocomposites, it is possible to form covalent bonds between BSA and SWCNT, which can be formed as a result of laser exposure to water-albumin dispersion of nanotubes.

The aim of this work was to study the nature of the interaction between single-walled carbon nanotubes and BSA based on the analysis of vibrational (Fourier-transform infrared (FTIR) and Raman spectroscopy) spectra of solid nanocomposites. For this, the vibrational spectra of nanocomposites based on BSA and SWCNT were interpreted depending on the concentration and diameter of nanotubes, and the mechanism of interaction of BSA with SWCNT was also determined. A quantum chemical calculation was performed to optimize the structure of SWCNT complex with the amino acid residues Lys (Lysine) and Glu (Glutamic) of albumin.

2. Experimental

2.1. Materials and preparation of composites

For the manufacture of water-protein dispersion with carbon nanotubes the most photo-resistant type of protein - bovine serum albumin (BSA) - was used. Albumin is widely used as a laser solder, which is put on laser-welded biological tissue [30–37]. The laser welding procedure is similar to the method of obtaining a nanocomposite in our work. For albumin, a typical conformation is a

secondary or tertiary one with a negligible protein burdening with toxic products. The picture of a dried drop of freshly prepared water-albumin dispersion is characterized by the presence of a significant number of radial cracks forming arches along the edge of the drop. It is well studied at the atomic-structural level: the albumin molecule has two modifications (isomers), representing an ellipsoid of rotation and an irregular triangular prism [38]. A bulk material was obtained from a water suspension of BSA with a concentration of ~25 wt% under laser irradiation. BSA was used as a bonding element for nanoparticles - carbon nanotubes.

Two types of single-walled carbon nanotubes (SWCNT) were used as fillers for the albumin matrix. The main difference between the types of nanotubes was their geometrical dimensions. Nanotubes of the first type (SWCNT I) were synthesized by the electric arc method on a Ni/Y catalyst, purified in a dispersion of HNO_3/H_2SO_4, with rinsing until neutral reaction after that. The average diameter of nanotubes is about 1.4–1.8 nm, length - 0.3–0.8 μm, specific surface area was ~400 m^2/g. The purity of the SWCNT was 98%. The nanotubes of the second type (SWCNT II) were obtained by gas-phase synthesis and purified with the use of a similar method as the first type of SWCNT I. The average diameter was 3.2–4 nm, their length was about 5 μm, and the specific surface area was 420 m^2/g. The degree of purity of SWCNT II was 91%.

SWCNT transmission electron microscopy images are shown in Fig. 1a and b. Nanotubes are in the form of single nanotubes and their bundles sizes up to 30 nm. It is known that their properties depend on the chirality. To determine the chirality of nanotubes, the method proposed by the authors of [39–41] was used. The performed RBM analysis of the Raman spectra and optical absorption spectra of SWCNT of both types [42,43] showed that the used SWCNTs are a mixture of chiral nanotubes. For SWCNT I, ~62% of such type had chirality (11.9), ~24% - (12.8) and ~14% - (11.10). SWCNT II had a wider range of chirality indices, main among them: (36.12), (33.16) and (28.19).

SWCNTs have the ability to stick together in bundles under the influence of van der Waals forces. For this, we use the technique of preparing a homogeneous water dispersion of SWCNT. To prepare the dispersion, nanotubes were dispersed in water using a powerful ultrasonic homogenizer (power about 40 W). Next, BSA (concentration about 25 wt%) was added to the water dispersion of nanotubes in a form of a powder and mixed using a magnetic stirrer, and then were placed in an ultrasonic bath with a power not more than 7 W. The interaction between SWCNT and albumin and the functionalization of nanotubes by BSA atoms leads to their maximum possible separation and homogeneous distribution of the tubes in the dispersion. BSA is a surfactant for SWCNT and inhibits the effect of “sticking” nanotubes. However, combining several SWCNTs in a bundle does not reduce the strength characteristics of composites [44].

The method of producing nanocomposites was as follows. First, the water-albumin dispersion was deposited on a silicon substrate, then it was irradiated with laser radiation (Fig. 2). To obtain a bulk sample, dispersion layers are applied and irradiated one after another. An alternative method for producing a bulk nanocomposite is to irradiate water-albumin dispersion in a bulk vessel, such as a Petri dish.

A diode laser with a generation wavelength of 810 nm was used for irradiation. The laser power was up to 3 W. In order to prevent a strong heating and denaturation of the protein during the preparation of nanocomposites, the temperature of the irradiated dispersion was controlled and maintained in the range of 60–80 °C. For this, a calibrated IR temperature sensor and a feedback system connecting the laser and the sensor were used. The denaturation temperature of the BSA was determined by differential scanning calorimetry and was about 85.7 °C. The laser irradiation was carried out until the water component of the dispersion was evaporated. As a result of irradiation, a nanocomposite was formed in the solid phase state (Fig. 1c). The concentration of nanotubes in the composite was about 0.01, 0.1 and 1 g/l. The specific surface area of the pores in the nanocomposites was about 280 m^2/g with their volume ~50%. Methods for preparing samples and studying their physicochemical properties of water dispersions and nanocomposites are described in detail in works [3,23–25].

2.2. FTIR and Raman measurements

Absorption spectra of the samples were recorded with the use of the Nicolet iS50 Thermo Scientific Fourier-transform spectrometer. IR absorption spectra were measured in the range of 500–4000 cm^{-1} at room temperature. Composite samples were crushed into fragments and KBr pellets were made from them. The thickness of the samples for IR spectroscopy was ~1 mm. The IR absorption spectra were averaged over 256 scans for each sample, and the spectral resolution was 1 cm^{-1}.

Raman spectra were obtained on the LabRAM HR Evolution HORIBA Scientific spectrometer. The spectra were excited by a semiconductor laser with a wavelength of 633 nm, power up to 0.5 W (depending on the signal-to-noise ratio) and a duration of 10 s. Spectra were measured at room temperature. The curves were averaged over 150 scans, recorded with a resolution of 1 cm^{-1}, and subjected to the inverse Fourier transform.

2.3. Quantum chemical study

Quantum chemical modeling and calculations were performed with the use of the DFT method at the B3LYP/6-31 g (d, p) level in the Gaussian-09 program. In order to stabilize the zwitterion in the solid phase, the reactive field model (Polarized Continuum Model, SCRF-PCM) was used. In this model, the cavity, in which the molecule under the study was placed, is a combination of overlapping van der Waals spheres constructed along the lines of isodensity.

2.4. In vitro investigation

For *in vitro* studies of nanocomposites, a human fibroblast cell line (FH-T), which was acquired at the National Research Center for Epidemiology and Microbiology of the Ministry of Health of the Russian Federation, was used. Cells were cultured in DMEM − 90% culture medium supplemented with 10% calf fetal serum in a 12 well plate. The FH-T cell concentration was approximately ~4×10^4 cells/ml. We studied samples of nanocomposites with two compositions. They differed in the type of nanotubes (SWCNT I and SWCNT II). The concentration of BSA in nanocomposites was ~25 wt % and the concentration of nanotubes was ~0.01 wt%. Nanocomposites were formed on a coverslip by a laser method. This nanocomposite coverslip was placed on the bottom of each well of a 12 well plate. A clean coverslip without a nanocomposite was used as a control. Next, a cell suspension was added to the each well of the plate. Cell cultivation on nanocomposites and control was carried out in a CO_2 incubator. A photocolorimetric MTT assay was used to assess the viability of cells grown on samples for 24 and 48 h. The MTT assay was carried out by determining the optical density with an Immunochem-2100 microplate photometer. The optical density was proportional to the number of living cells. The culture medium was removed from the plate wells after a cultivation period (24 or 48 h). 100 μl of pure culture medium with 20 μl of MTT at an initial concentration of 5 mg/ml was added to the each well. Then, MTT cells were kept for 2 h in a CO_2 thermostat. Next, MTT culture medium was removed and dimethyl sulfoxide 100 μl was added to the each well. It was necessary for the dissolution of formazan which was restored by the cells. Then, the cell pellet was resuspended for 10 min, and the absorbance was measured at a

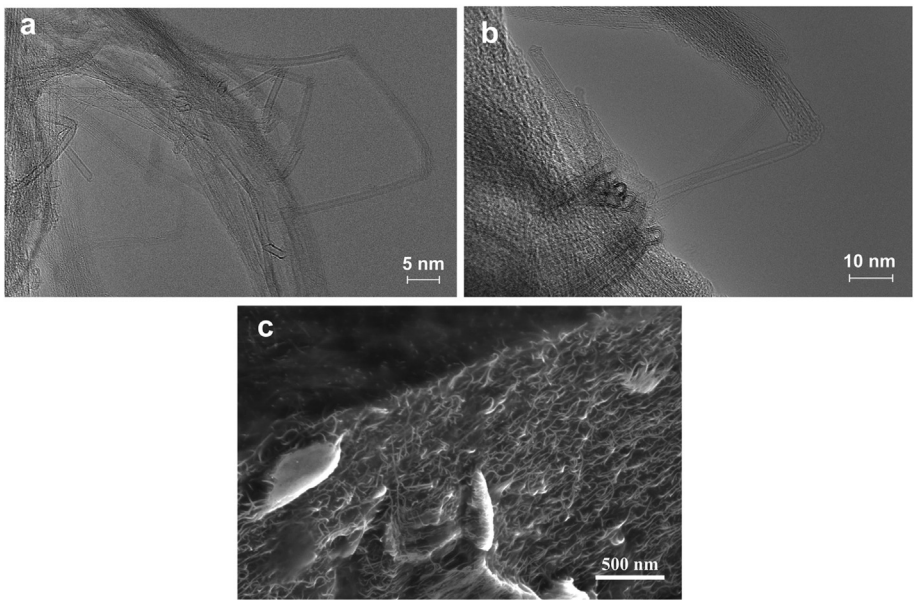

Fig. 1. Transmission electron microscopy images of small SWCNT I (a) and large SWCNT II (b) and scanning electron microscopy image of cleaved nanocomposite based on BSA and SWCNT I with a concentration 1 g/l on a silicon substrate (c).

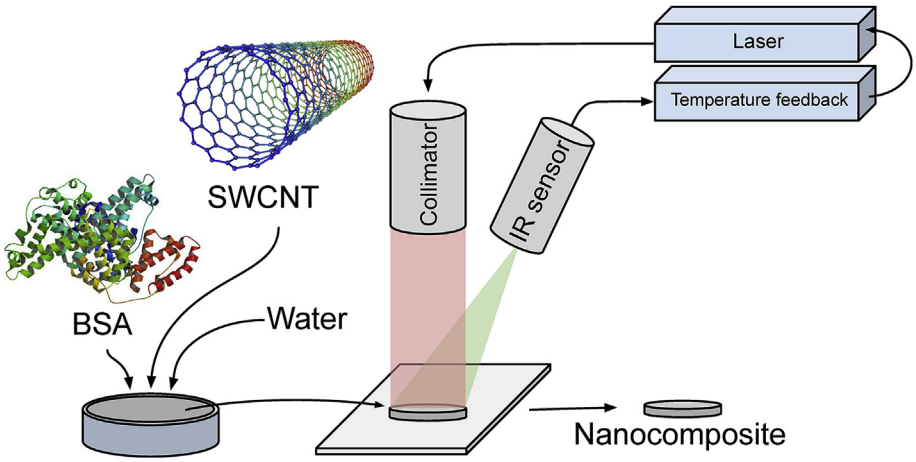

Fig. 2. The creation scheme of the SWCNT-based composites in BSA matrix.

wavelength of 492 nm. Cell viability was calculated as the percentage of grown cells on nanocomposites relative to the number of cells grown on the control.

Scanning electron microscopy was used to study the morphology of cells on nanocomposites. For this, nanocomposites were formed on silicon substrates of the same shape as the cover glass. Next, the cells were cultured as for the MTT assay. After incubation of the cells on the samples, the culture medium was removed. The cells were fixed in 2.5% glutaraldehyde for 30 min. Then the samples were washed in phosphate buffer for 2 min. At the end, the samples with cells in ethanol solutions with increasing concentration (50, 70, and 96%) were kept for dehydration.

3. Results and discussion

3.1. The quantum-chemical study of the interaction between BSA and SWCNT

It is known that the amino acid residues glutamic (Glu) and aspartic (Asp) are polar and have a negative charge at physiological pH values. In the radicals of acidic amino acids there is an additional carboxyl group. This group can form a chemical bond not only with the side chains of other amino acids, forming the tertiary structure of proteins. The carboxyl group can chemically bind to external molecular structures. The carboxyl groups of the amino acid residues Glu and Asp, most of which are located on the outer surface of the protein molecule, are distinguished on the structure. In Fig. 3 the molecular structure of one of the BSA domains is showed. In the figure, the red and blue colors denote the atoms of oxygen and nitrogen, respectively. It is known that carbon nanotubes can be functionalized by oxygen atoms [45–47]. The amino acids Glu and Asp, which have a negative charge: O_2CCH_2-, $-O_2CCH_2CH_2-$, are the only amino acid residues, which are capable of functionalizing SWCNT. Other amino acids which have positively charged or neutral amino acid residues do not participate in the functionalization of nanotubes. This is due to the features of the π-electronic structure of SWCNT.

To determine the nature of the interaction between BSA and SWCNT, the calculation was done. The structural fragment of the amino acid residues Asp and Glu was chosen as a molecular model

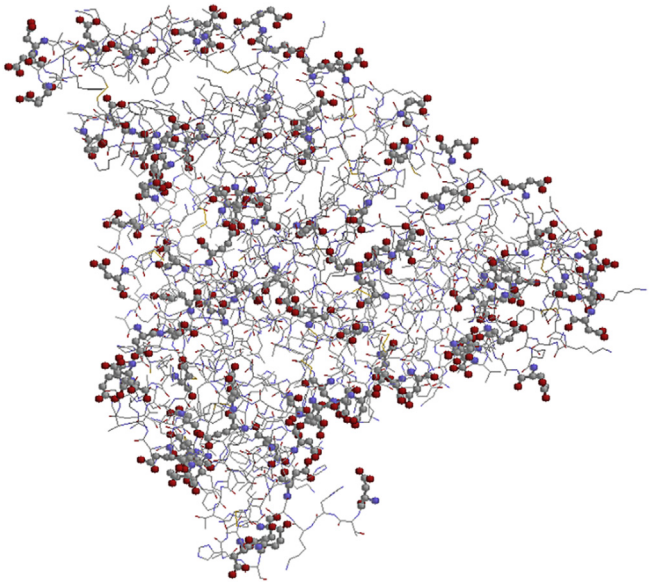

Fig. 3. The structure of BSA domain with the designation of carboxyl groups in Glu and Asp (red color - oxygen, blue color – nitrogen).

which interacts with SWCNT (Fig. 4a–c). The fragment had a negative charge. According to the results of the calculation, this structural fragment of amino acid residues Asp and Glu forms a covalent bond $C_{SWCNT}O$ (Fig. 4 d). The energy of this covalent bond was 580 kJ/mol, and the bond length was 1.42 Å (nanotube diameter is 1.7 nm).

Laser irradiation of the water-albumin dispersion of SWCNT can lead to the initiation of a chemical reaction between the negatively charged amino acid residues Asp and Glu and nanotubes and, respectively, the formation of covalent bonds between them. This is due to the peculiarity of the formation of a composite structure in the solid phase state by laser radiation during temperature control.

3.2. Analysis of the vibrational spectra of nanocomposites

The vibrational spectra of BSA have been the subject of a number of experimental and theoretical studies [38,48–53]. The works

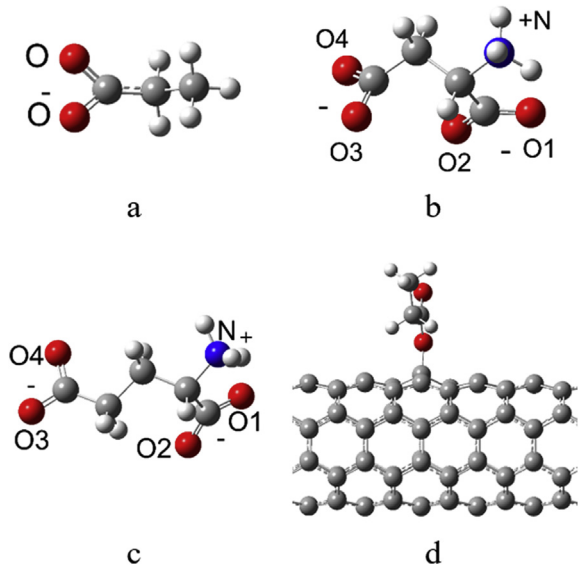

Fig. 4. Molecular fragment (a) entering into the side chain of Asp (b) and Glu (c) and forming a covalent bond with the SWCNT (d).

demonstrated that in the spectrum of albumin, as well as other proteins, it is possible to distinguish the characteristic vibrations of the amide group of polypeptides. These are vibrations with a frequency near 1650 cm^{-1} and 1540 cm^{-1}. The shape of the oscillation near 1650 cm^{-1} is mainly determined by the change in the length of the C=O peptide bond. For vibrations with a frequency near 1540 cm^{-1}, the shape is mixed and determined by changes in the angle of CNN and the bond length of CN. These oscillations are commonly called oscillations Amide I and Amide II, respectively.

Analysis of the frequencies and intensities of the absorption bands and lines of the Raman vibrations of the amide group is widely used to establish the conformational structure of the polypeptide chain. For example, a comparative analysis of the vibrational spectra of ovalbumin and S-ovalbumin in the region of 800–1850 cm^{-1} was performed in work [38]. The difference between the spectra made it possible to establish quantitative characteristics of the relative abundance of the β-folded and α-spiral structure of these two albumin analogs similar in structure.

Determining the formation of a covalent bond between SWCNT and Asp and Glu amino acid residues requires a more detailed interpretation of the vibrational spectra of BSA. For this, experimental measurements of the FTIR and Raman spectra of BSA were performed and the vibrational spectra of the zwitterionic forms of 20 amino acids and their dipeptides were calculated [54]. It has been established that the vibrational forms of the side amino acid residues forming the polypeptide do not mix with the vibrational forms of the amide moiety (Amide I, Amide II and Amide III). This allows them to be used to interpret the vibrational FTIR and Raman spectra of BSA. A comparison between experimental and calculated [54] BSA spectra showed that each experimental albumin absorption band is a superposition of several absorption bands of side amino acid residues. At the same time, the effect of intermolecular interactions between amino acid residues leads to a shift of the maximum and a change in the intensity of the absorption bands corresponding to the vibrations of Amide I, Amide II and Amide III. The overlapping of the absorption bands of amino acid residues with the absorption band of Amide I makes it very sensitive to the structural changes. In particular, the absorption band Amide I is sensitive to the manifestation of intermolecular interactions, as a result of which a shift in the frequency and intensity of this band makes it possible to determine the structural changes in the protein. An analysis of the intensity of the vibrational spectra of amino acid residues in the region of 1540 cm^{-1} showed that intermolecular interactions lead to a more significant change in the intensity of the absorption band of the Amide II in the FTIR spectrum compared to the Raman spectrum. In the region of the Amide III oscillation (about 1300–1200 cm^{-1}), the deformated δ (OH) and δ (NH) vibrations of the side chains of a number of amino acids, which are involved in intermolecular interaction, appeared. As a result, the values of the corresponding frequencies of the deformation oscillations of Amide III can shift. In addition, a broad absorption band of average intensity appeared in the experimental FTIR spectrum of BSA in the region of ~660 cm^{-1}. According to the calculation, in this spectral range, the deformation oscillations of the angles γ (CCO), γ (COC) and γ (OCO-) amino acid residues Glu and Asp appeared. The participation of Glu and Asp in the intermolecular interaction with other amino acid residues led to a shift in the oscillation frequency of a given deformation vibration and the broadening of the corresponding absorption band.

Fig. 5 shows the experimental IR spectra of BSA and solid nanocomposites with different SWCNT I concentrations 0.01, 0.1 and 1 g/l.

The interaction between the negatively charged oxygen group COO - protein residues Asp and Glu and carbon atoms (C_{CNT}) led to the formation of covalent bonds C_{SWCNT}-O and bond angles $C_{SWCNT}OO$. This affected the values of the oscillation frequencies

and the intensities of the absorption bands in the range of oscillations Amide I, Amide II, and also in the range of 650 cm^{-1}, which is observed in the spectra of solid nanocomposites with different SWCNT concentrations (Fig. 6).

Comparing the FTIR spectra of nanocomposites at different concentrations of nanotubes demonstrated that each spectrum is a superposition of two spectra — with and without the formation of covalent bonds (Fig. 5b — d). It is obvious that an increase of the nanotubes concentration led to the saturation of the functionalization of SWCNT with oxygen atoms of amino acid residues Asp and Glu. In the total spectrum, at the concentration of nanotubes 1 g/l, the spectrum of BSA prevails.

An increase in the tubes diameter (from 1.7 to 4 nm) in the nanocomposite did not led to a significant change in the FTIR spectrum, as it was in comparison with the BSA spectrum and in comparison with the spectra of nanocomposites with different concentrations of nanotubes. This is due to the steric factor that complicates the interaction of albumin with nanotubes through the formation of covalent bonds. Small changes observed in the spectra of nanocomposites with an increase in the nanotubes concentration from 0.01 to 1 g/l demonstrated that isolated cases of covalent attachment of albumin to nanotubes of larger diameter are not excluded (Fig. 6).

An important spectral range for studying the interaction of BSA with SWCNT is the high-frequency range (2700-3600 cm^{-1}). To determine the effect of intermolecular interactions on the vibrational spectra of proteins, we calculated the structure and vibrational spectra of the Gly:Gly (Glycine:Glycine), Glu:Thr (Glutamic acid:Threonine) and Asp:Lys (Aspartic acid:Lysine)complexes. This made it possible to take into account three types of intermolecular interactions — hydrogen, ion–dipole, and ion–ion bonds (Fig. 7). These types of bonds can be used to qualitatively evaluation of the intermolecular interactions between the neutral and charged side chain groups Rm–OH … COO (−)-Rn and between the charged side chain groups inside the protein molecule Rm–NH3 + … COO (−)-Rn.

According to the calculation, the energy of the intermolecular interaction varied in a wide range - from 8 to 315 kJ/mol (Table 1).

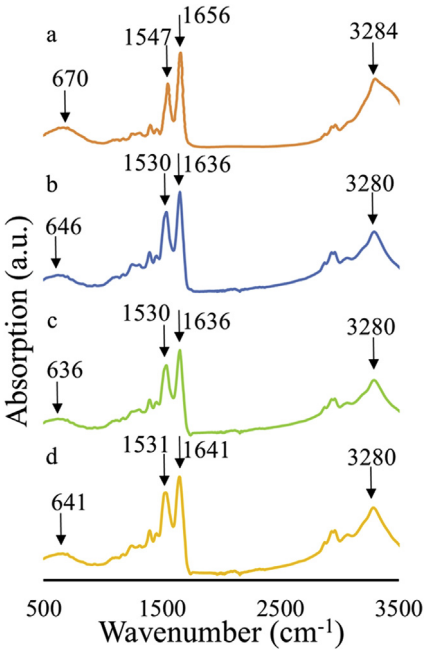

Fig. 5. FTIR spectra of BSA (a) and BSA solid nanocomposites with SWCNT I with a concentration of 0.01 (b), 0.1 (c), 1 (d) g/l.

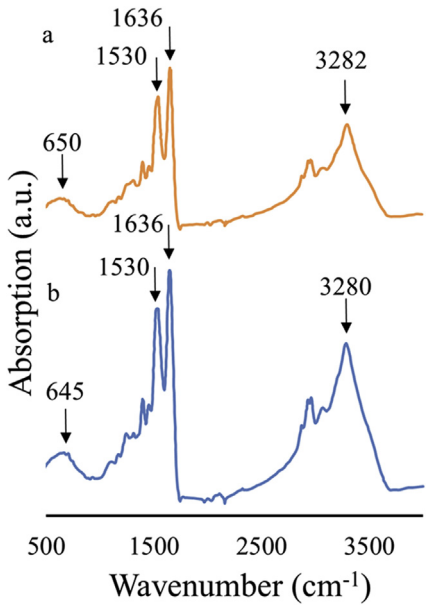

Fig. 6. FTIR spectra of BSA nanocomposites with SWCNT II with a concentration of 0.01 (a) and 0.1 (b) g/l.

The magnitude of the oscillation frequency shifted when the intermolecular bond was broken also varied widely from 50 to ~400 cm^{-1}, and the intensity of the IR absorption bands and the Raman bands of the spectrum could decrease by 100 times. In Table 1, the frequencies of valence vibrations of NH and $N^{+}H$ before and after breaking of intermolecular bonds are denoted by ν_1 and ν_2, respectively. In parentheses are the intensities of the IR (km/mol) and Raman ($Å^4$/AMU) bands.

A significant decrease in the intensities of the experimental absorption bands of nanocomposites for different concentrations of nanotubes (Fig. 5), as well as a shift in the frequencies of stretching vibrations in the high-frequency region, showed that conformational changes occur under the influence of laser radiation on the water-albumin dispersion with SWCNT I (with a small diameter 1.7 nm) in the secondary and tertiary structures of BSA. For SWCNT II (with a large diameter 4 nm), such characteristic changes were not observed.

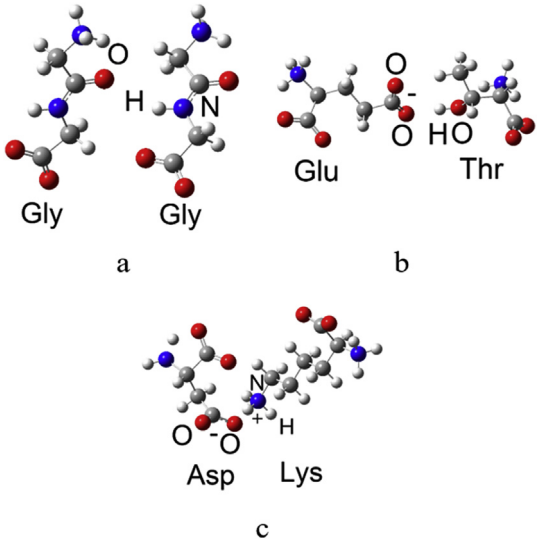

Fig. 7. Molecular structures forming hydrogen Gly: Gly (a), ion-dipole Glu: Thr (b) and ion-ion Asp: Lys (c) intermolecular bonds in albumin.

Table 1
The energy of intermolecular interaction (E) and frequency (ν, cm^{-1}) of valence vibrational bonds.

Structure	Bond	E, (kJ/mol)	Oscillation frequency and intensity		
			ν_1, cm^{-1} (km/mol; Å^4/AMU)	ν_2, cm^{-1}, (km/mol; Å^4/AMU)	Ratio
Gly:Gly	O…HN	8	3412 (361; 36)	3462 (321; 17)	q(NH) Gly
Glu:Thr	$(COO)^-$ … (OH)	133	3420 (282; 1287)	3831 (89; 163)	q(OH) Thr
Asp-Lys	$(COO)^-$ … (N^+H_3)	315	3126(1964; 59)	3428 (54; 147)	q(N^+H_3) Lys

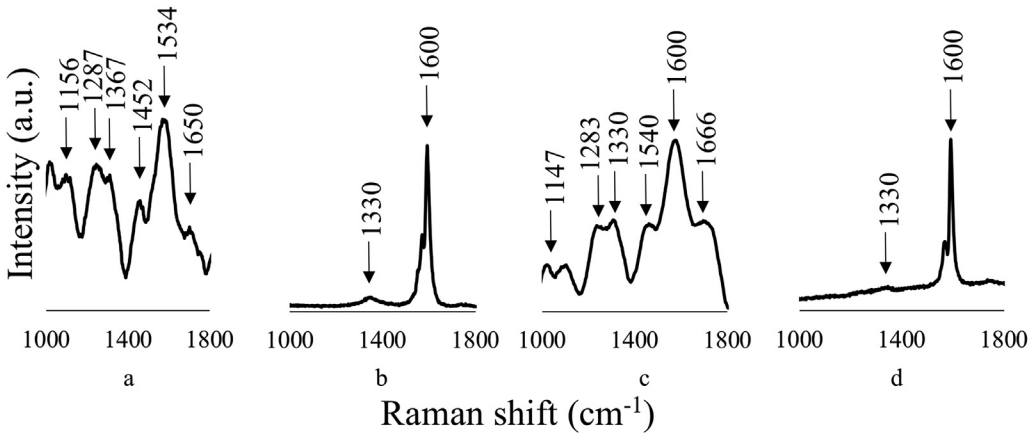

Fig. 8. Raman spectra for BSA (a), SWCNT I (b) and BSA nanocomposites with SWCNT I with a concentration of 0.01 (c) and 1 (d) g/l.

Obviously, the formation of covalent bonds should also appear in the Raman spectra of SWCNT. It should be noticed that for an ideal (defect-free) nanotube in the Raman spectrum, radial-breathing (low-frequency region ~ 200 cm^{-1}) and tangential (high-frequency region ~ 1600 cm^{-1}) vibrations appeare. In the range of 1300 cm^{-1} (D-band) there is a line induced by the presence of various types of defects caused by the imperfection of the nanotube lattice and the presence of impurities [55]. Other modes have very low intensity and are practically not observed in the Raman spectrum.

Defects can be caused by imperfections in the lattice as a result of the synthesis of nanotubes or exposure by external fields (for example, exposure by laser radiation), as well as the presence of impurities, which also include the formation of covalent bonds with oxygen atoms. The G + D or G' + D bands are also very sensitive to defects in SWCNT. By their displacement relative to the G or G' bands, one can judge the manifestation of the semiconductor or metallic properties of nanotubes. The 2D band, which appears in the range of 2700 cm^{-1}, also allows one to judge defects that arise in nanotubes. The ratio of G and D bands helps to find out what is the magnitude of the defect. For more advanced nanotubes, the D band is several times of magnitude smaller than the G band. If the intensities of these bands are proportional, this indicates a rather large number of defects in nanotubes. Therefore, if in the spectrum of SWCNT while interacting with a biological object in the vibration region of the G, D bands, their overtones and composite frequencies, frequency shifts and a change in intensity are observed, this is a sign of the formation of SWCNT defects, including those caused by functionalization.

In Fig. 8 the Raman spectra of pure BSA, SWCNT I and solid nanocomposite with SWCNT I, the concentration of which was 0.01 and 1 g/l, are showed.

In the experimental spectrum of the single-walled carbon nanotubes, the intensity of the Raman band in the range of ~1330 cm^{-1} is substantially less than the intensity of the band of 1600 cm^{-1}, which indicates the high purity of the used nanotubes.

In the Raman spectrum of the nanocomposite with a low concentration of nanotubes (0.01 g/l), a significant increase in the band intensity was observed in the range of ~1330 cm^{-1}. Thus, the intensity of the band in the range of ~1330 cm^{-1} becomes comparable with the intensity of the band in the range of ~1600 cm^{-1} (Fig. 8c). This confirms the presence of a significant number of defects in the SWCNT as a part of the composite. The defects were caused by a covalent addition of oxygen to the graphene surface of nanotubes. Raman spectra of the nanocomposites at different concentrations of nanotubes were a superposition of two spectra - with the formation and without the formation of covalent bonds (Fig. 8). An increase in the concentration of nanotubes led to the saturation of the functionalization of SWCNT with oxygen atoms of the amino acid residues Asp and Glu. This is confirmed by the fact that in the total spectrum of the nanocomposite with a high concentration of nanotubes 1 g/l, the Raman spectrum of SWCNT prevails.

3.3. Cell viability on nanocomposites

To determine the possibility of using nanocomposites to create scaffolds and tissue-engineering matrices, a series of *in vitro* experiments was performed. We have studied the viability of fibroblast connective tissue cells (FH-T) on nanocomposites formed on a

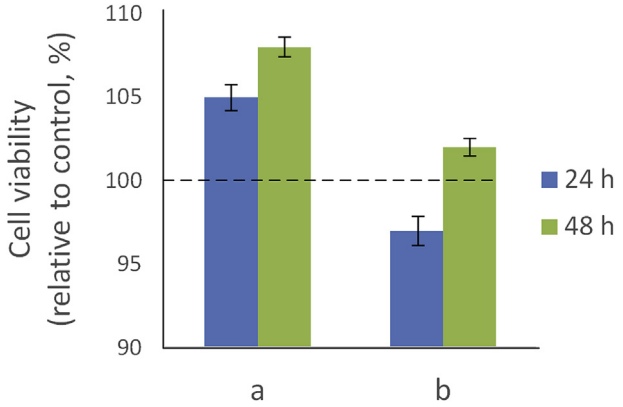

Fig. 9. Cell viability on nanocomposites based on BSA and SWCNT I (a) or SWCNT II (b) relative to the control sample in 24 and 48 h after the start of cultivation.

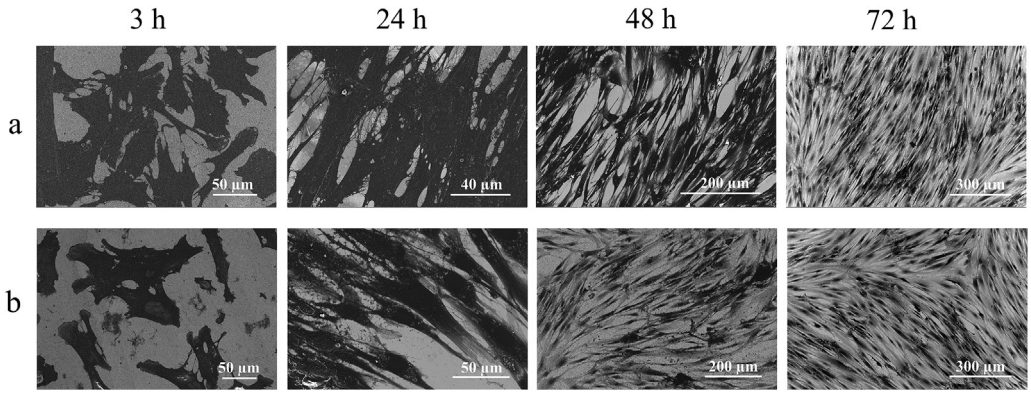

Fig. 10. SEM image of fibroblasts on nanocomposites based on BSA and SWCNT I (a) or SWCNT II (b) in 3, 24, 48 and 72 h after the start of cultivation.

coverslip in comparison with a control (clean coverslip). The results of the MTT assay after cell culture are shown in Fig. 9. 24 h after the start of cultivation, the best cell survival was demonstrated on a nanocomposite with SWCNT I (4.5% higher than in the control). Cell survival on the nanocomposite of SWCNT II was slightly lower than the control (3%). After 48 h, the cell survival trend for the nanocomposite based on SWCNT I continued. The value exceeded the control by more than 7%. Cell growth on a nanocomposite of SWCNT II slightly exceeded the control value after 48 h (2%).

The study of the fibroblasts morphology on nanocomposites at various time intervals was carried out with the use of scanning electron microscopy (SEM) (Fig. 10). The SEM image demonstrated the growth, extension, and spreading of cells on the surface of samples over time. 3 h after the start of cultivation, the cells partially retain a rounded shape, which indicates the incompleteness of the process of attachment of cells to the surface of the samples. After 24 h, the cells are elongated, they became oblong, and their area was significantly increased. Cell nuclei and pseudopodia were visible in the images, with the help of which the cells were attached to the surface of the nanocomposite. After 72 h of incubation, the cells completely filled the nanocomposite surface. However, after 72 h, the better effect of the nanocomposite based on SWCNT I on cell growth was noticeable. Fibroblasts lined up to form a monolayer. This may be due to the best compatibility of the nanocomposite structure with the fibroblasts, which led to better adhesion of cells to the surface of the nanocomposite based on SWCNT I.

4. Conclusions

In this work, the mechanism of the interaction between BSA with SWCNT in solid nanocomposites obtained by evaporating the water-albumin dispersion with nanotubes by a diode laser with temperature control was investigated. Such nanocomposites can be used for creating cellular and tissue-engineering matrixes and laser welding of biological tissues with the use of water-protein dispersions with nanoparticles as a solder.

The possibility of nanotubes functionalization by oxygen atoms of negative amino acid residues Asp and Glu, which are on the outer surface of BSA, was shown by molecular modeling. The formation of covalent bonds between BSA and SWCNT was confirmed by FTIR and Raman spectra, which were recorded for nanotubes of small diameter (1.7 nm) with different concentrations (0.01, 0.1 and 1 g/l). The comparison of the IR spectra of the nanocomposites of different nanotubes concentrations showed that each spectrum is a superposition of two spectra — with and without the formation of covalent bonds. An increase in the concentration of nanotubes led to the saturation of the functionalization of SWCNT with oxygen atoms of the amino acid residues Asp and Glu. In the total spectrum of the nanocomposite with a SWCNT concentration 1 g/l, the BSA spectrum prevails.

The covalent interaction between BSA with SWCNT led to the disruption of the secondary and tertiary structures of albumin, as evidenced by a significant decrease in the intensity of the absorption bands in the high-frequency range. According to the calculation of the vibrational spectra of the three Gly: Gly, Glu: Thr and Asp: Lys complexes, which allow to take into account hydrogen, ion-dipole and ion-ion bonds, a significant decrease in the intensity of absorption bands in the region of stretching bond oscillations in the intermolecular interaction OH and NH was observed.

The formation of a covalent bond between BSA and SWCNT in the nanocomposite led to an increase in the intensity of the band in the range of ~1330 cm^{-1} on the Raman spectrum compared to the spectrum of the original nanotubes. This confirms the presence of significant defects in SWCNT caused by covalent addition of oxygen to the graphene surface of nanotubes.

It was found that an increase in the diameter of nanotubes and their concentration in the nanocomposite have practically no effect on the vibrational spectra, which confirms the hydrophobic interaction between BSA and SWCNT.

In this way, two types of interactions in the solid BSA-based nanocomposites with SWCNT — hydrophobic and with the formation of covalent bonds — depend on the diameter of the nanotubes used. The viability of fibroblast connective tissue cells on nanocomposites with both types of SWCNT was demonstrated. It was found that nanocomposites based on SWCNT I provided slightly better compatibility of their structure with fibroblasts. It allows achieving better cell adhesion to the nanocomposite surface. Thus, laser-formed nanocomposites from BSA and SWCNT can be used to create cell scaffolds and tissue-engineering matrices.

Declaration of competing InterestCOI

The authors declare that they have no known competing financial interests or personal relationships that could have appeared to influence the work reported in this paper.

Acknowledgements

This study was supported by the Russian Science Foundation, project no. 18-79-10008 and Russian academic excellence project "5–100″ for Sechenov First Moscow State Medical University. The studies were performed using MIET Core facilities center "MEMS and electronic components". The authors are grateful for the helpful discussions of Yu. Shaman, E. Kitsyuk., P. Vasilevsky, and Yu. Fedorova.

References

[1] L.P. Zanello, B. Zhao, H. Hu, R.C. Haddon, Bone cell proliferation on carbon nanotubes, Nano Lett. 6 (3) (2006) 562–567, https://doi.org/10.1021/nl051861e.

[2] E. Hirata, M. Uo, Y. Nodasaka, H. Takita, N. Ushijima, T. Akasaka, F. Watari, A. Yokoyama, 3D collagen scaffolds coated with multiwalled carbon nanotubes: initial cell attachment to internal surface, J. Biomed. Mater. Res. B Appl. Biomater. 93B (2) (2010) 544–550, https://doi.org/10.1002/jbm.b.31613.

[3] A. Yu Gerasimenko, L.P. Ichkitidze, V.M. Podgaetsky, S.V. Selishchev, Biomedical applications of promising nanomaterials with carbon nanotubes, Biomed. Eng. 48 (6) (2015) 310–314, https://doi.org/10.1007/s10527-015-9476-z.

[4] A. Wesełucha-Birczyńskaa, K. Morajkaa, E. Stodolak-Zychb, E. Długońb, M. Dużyjac, Tomasz Lisb, Maciej Gubernatb, Magdalena Ziąbkab, Marta Błażewiczb, Raman studies of the interactions of fibrous carbon nanomaterials with albumin, Spectrochim. Acta 196 (2018) 262–267, https://doi.org/10.1016/j.saa.2018.02.027.

[5] R.S.A. Sonthanasamy, N.M.N. Sulaiman, L.L. Tan, A.M. Lazim, Comprehensive spectroscopic studies of synergism between Gadong starch based carbon dots and bovine serum albumin, Spectrochim. Acta 218 (2019) 85–96, https://doi.org/10.1016/j.saa.2019.03.108.

[6] L. Carson, K. Hibbert, F. Akindoju, C. Johnson, M. Stewart, C. Kelly-Brown, G. Beharie, T. Fisher, J. Stone, D. Stoddart, A. Oki, G.M. Neelgund, G. Regisford, P. Traisawatwong, J. Zhou, Z. Luo, Synthesis, characterization and stability of chitosan and poly(methylmethacrylate) grafted carbon nanotubes, Spectrochim. Acta 96 (2012) 380–386, https://doi.org/10.1016/j.saa.2012.05.042.

[7] G.I. Dovbeshko, O.M. Fesenko, E.D. Obraztsova, K.R. Allakhverdiev, A.E. Kaja, Conformation analysis of nucleic acids and proteins adsorbed on single-shell carbon nanotubes, J. Struct. Chem. 50 (5) (2009) 954–961, https://doi.org/10.1007/s10947-009-0142-8.

[8] B.D. Holt, K.N. Dahl, M.F. Islam, Quantification of uptake and localization of bovine serum albumin-stabilized single-wall carbon nanotubes in different human cell types, Small 7 (16) (2011) 2348, https://doi.org/10.1002/smll.201100437.

[9] L. Li, R. Lin, H. He, L. Jiang, M. Gao, Interaction of carboxylated single-walled carbon nanotubes with bovine serum albumin, Spectrochim. Acta, Part A 105 (2013) 45–51, https://doi.org/10.1016/j.saa.2012.11.111.

[10] F. Lu, L. Gu M.J. Meziani, X. Wang, P.G. Luo, L. Monica, V. Cao, Y.-P. Sun, Advances in bioapplications of carbon nanotubes, Adv. Mater. 21 (2) (2009) 139–152, https://doi.org/10.1002/adma.200801491.

[11] N. Thamwattana, D. Baowan, B.J. Cox, Interaction of carboxylated single-walled carbon nanotubes with bovine serum albumin, RSC Adv. 3 (2013) 23482–23488, https://doi.org/10.1039/C3RA43991G.

[12] T. Kopac, K. Bozgeyik, Equilibrium, kinetics, and thermodynamics of bovine serum albumin adsorption on single-walled carbon nanotubes, Chem. Eng. Commun. 203 (9) (2016) 1198–1206, https://doi.org/10.1080/00986445.2016.1160225.

[13] L. Muzi, F. Tardani, C. La Mesa, A. Bonincontro, A. Bianco, G. Risuleo, Interactions and effects of BSA-functionalized single-walled carbon nanotubes on different cell lines, Nanotechnology 27 (15) (2016), https://doi.org/10.1088/0957-4484/27/15/155704, 155704.

[14] Y. Guan, H. Zhang, Y. Wang, New insight into the binding interaction of hydroxylated carbon nanotubes with bovine serum albumin, Spectrochim. Acta 124 (2014) 556–563, https://doi.org/10.1016/j.saa.2014.01.058.

[15] Y. Hai, K. Qu, Y. Liu, C. Zhao, Binding mechanism of single-walled carbon nanotubes (SWCNTs) to serum albumin: spectroscopy and molecular modelling exploration, Environ. Chem. 15 (5) (2018) 278–285, https://doi.org/10.1071/EN18043.

[16] S. Erbis, Z. Ok, J.A. Isaacs, J.C. Benneyan, S. Kamarthi, Review of research trends and methods in nano environmental, Health, and safety risk analysis, Risk Anal. 36 (2016) 1644–1665, https://doi.org/10.1111/risa.12546.

[17] B.S. Harrison, A. Atala, Carbon nanotube Applications for tissue engineering, Biomaterials 28 (2) (2007) 344–353, https://doi.org/10.1016/j.biomaterials.2006.07.044.

[18] N.O. Chahine, N.M. Collette, C.B. Thomas, D.C. Genetos, G.G. Loots, Nanocomposite scaffold for chondrocyte growth and cartilage tissue engineering: effects of carbon nanotube surface functionalization, Tissue Eng. A 20 (2014) 17–18, https://doi.org/10.1089/ten.TEA.2013.0328.

[19] T. Trzeciak, J.D. Rybka, E. Me Akinoglu, M. Richter, J. Kaczmarczyk, M. Giersig, Vitro evaluation of carbon nanotube-based scaffolds for cartilage tissue engineering, J. Nanosci. Nanotechnol. 16 (2016) 9022–9025, https://doi.org/10.1166/jnn.2016.12733.

[20] L. Pan, X. Pei, R. He, Q. Wan, J. Wang, Multiwall carbon nanotubes/polycaprolactone composites for bone tissue engineering application, Colloids Surf., B 93 (2012) 226–234, https://doi.org/10.1016/j.colsurfb.2012.01.011.

[21] J.N. Mackle, D.J. Bond, E. Mooney, C. McDonnell, W.J. Blau, G. Shaw, F.P. Barry, J.M. Murphy, V. Barron, In vitro characterization of an electroactive carbon-nanotube-based nanofiber scaffold for tissue engineering, Macromol. Biosci. 11 (2011) 1272–1282, https://doi.org/10.1002/mabi.201100029.

[22] D. Naskar, A.K. Ghosh, M. Mandal, P. Das, S.K. Nandi, S.C. Kundu, Dual growth factor loaded nonmulberry silk fibroin/carbon nanofiber composite 3D scaffolds for in vitro and in vivo bone regeneration, Biomaterials 136 (2017) 67–85, https://doi.org/10.1016/j.biomaterials.2017.05.014.

[23] A. Yu Gerasimenko, A.A. Dedkova, L.P. Ichkitidze, V.M. Podgaetskii, S.V. Selishchev, A study of preparation techniques and properties of bulk nanocomposites based on aqueous albumin dispersion, Opt Spectrosc. 115 (2013) 283–289, https://doi.org/10.1134/S0030400X13080092.

[24] L.P. Ichkitidze, A.Yu Gerasimenko, V.M. Podgaetsky, S.V. Selishchev, Layers with the tensoresistive properties and their possible applications in medicine, Mater. Phys. Mech. 37 (2) (2018) 153–158, https://doi.org/10.18720/MPM.3722018_7.

[25] M.S. Savelyev, P.N. Vasilevsky, A. Yu Gerasimenko, L.P. Ichkitidze, V.M. Podgaetsky, S.V. Selishchev, Nonlinear optical characteristics of albumin and collagen dispersions with single-walled carbon nanotubes, Mater. Phys. Mech. 37 (2018) 133–139, https://doi.org/10.18720/MPM.3722018_4.

[26] A. Yu Gerasimenko, O.E. Glukhova, G.V. Savostyanov, V.M. Podgaetsky, Laser structuring of carbon nanotubes in the albumin matrix for the creation of composite biostructures, J. Biomed. Opt. 22 (6) (2017), https://doi.org/10.1117/1.JBO.22.6.065003, 065003-1 - 065003-8.

[27] A. Yu Gerasimenko, E.P. Kitsyuk, A.V. Kuksin, R.M. Ryazanov, A.I. Savitskiy, M.S. Saveliev, A.A. Pavlov, Influence of laser structuring and barium nitrate treatment on morphology and electrophysical characteristics of vertically aligned carbon nanotube arrays, Diam. Relat. Mater. 96 (2019) 104–111, https://doi.org/10.1016/j.diamond.2019.04.035.

[28] A.Y. Gerasimenko, L.P. Ichkitidze, E.S. Piyankov, I.V. Pyanov, I.B. Rimshan, D.I. Ryabkin, M.S. Savelyev, V.M. Podgaetskii, Use of indocyanine green in nanocomposite solders to increase strength and homogeneity in laser welding of tendons, Biomed. Eng. 50 (5) (2017) 310–313, https://doi.org/10.1007/s10527-017-9644-4.

[29] I.B. Rimshan, N.N. Zhurbina, U.E. Kurilova, D.I. Ryabkin, A.Y. Gerasimenko, Biocompatible nanomaterial for restoration of continuity of dissected biological tissues, Biomed. Eng. 52 (1) (2018) 23–26, https://doi.org/10.1007/s10527-018-9774-3.

[30] I. Gabay, I. Barequet, D. Varssano, M. Rosner, A. Katzir, Bonding surgical incisions using a temperature-controlled laser system based on a single infrared fiber, J. Biomed. Opt. 18 (2013), https://doi.org/10.1117/1.JBO.18.11.111416, 111416-1–111416-5.

[31] L. Hu, Z. Lu, B. Wang, J. Cao, X. Ma, Z. Tian, Z. Gao, L. Qin, X. Wu, Y. Liu, L. Wang, Closure of skin incisions by laser-welding with a combination of two near-infrared diode lasers: preliminary study for determination of optimal parameters, J. Biomed. Opt. 16 (2011), https://doi.org/10.1117/1.3552648, 38001. 038001-1 – 038001-7.

[32] H.E. Savage, R.K. Halder, U. Kartazayeu, R.B. Rosen, T. Gayen, S.A. McCormick, N.S. Patel, A. Katz, H.D. Perry, M. Paul, R.R. Alfano, NIR laser tissue welding of in vitro porcine cornea and sclera tissue, Lasers Surg. Med. 35 (2004) 293–303, https://doi.org/10.1002/lsm.20094.

[33] D. Spector, Y. Rabi, I. Vasserman, A. Hardy, J. Klausner, M. Rabau, A. Katzir, In vitro large diameter bowel anastomosis using a temperature controlled laser tissue soldering system and albumin stent, Lasers Surg. Med. 41 (2009) 504–508, https://doi.org/10.1002/lsm.20799.

[34] A. Bregy, S. Bogni, V. Bernau, I. Vajtai, F. Vollbach, A. Petri-Fink, M. Constantinescu, H. Hofmann, M. Frenz, M. Reinert, Solder doped polycaprolactone scaffold enables reproducible laser tissue soldering, Lasers Surg. Med. 40 (2008) 716–725, https://doi.org/10.1002/lsm.20710.

[35] K. Tal, E. Strassmann, N. Loya, A. Ravid, N. Kariv, D. Weinberger, A. Katzir, D. Gaton, Corneal cut closure using temperature-controlled CO^2 laser soldering system, Lasers Med. Sci. 30 (2015) 1367–1371, https://doi.org/10.1007/s10103-015-1737-2.

[36] D. Simhon, I. Gabay, G. Shpolyansky, T. Vasilyev, I. Nur, R. Meidler, O. Hatoum, A. Katzir, M. Hashmonai, D. Kopelman, Temperature-controlled laser-soldering system and its clinical application for bonding skin incisions, J. Biomed. Opt. 20 (12) (2015), https://doi.org/10.1117/1.JBO.20.12.128002, 128002-1–128002-8.

[37] C.B. Bleustein, D. Felsen, D.P. Poppas, Welding characteristics of different albumin species with and without fatty acids, Lasers Surg. Med. 27 (2) (2000) 82–86, https://doi.org/10.1002/1096-9101(2000)27:1<82::AID-LSM11>3.0.CO;2-2.

[38] S. Kint, Y. Tomimatsu, A Raman difference spectroscopic investigation of ovalbumin and S-ovalbumin, Biopolimers 18 (1979) 1073–1079, https://doi.org/10.1002/bip.1979.360180505.

[39] H. Kataura, Y. Kumazawa, Y. Maniwa, I. Umezu, S. Suzuki, Y. Ohtsuka, Y. Achiba, Optical properties of single-wall carbon nanotubes, Synth. Met. 103 (1999) 2555–2558, https://doi.org/10.1016/S0379-6779(98)00278-1.

[40] H. Telg, J. Maultzsch, S. Reich, F. Hennrich, C. Thomsen, Chirality distribution and transition energies of carbon nanotubes, Phys. Rev. 93 (2004), https://doi.org/10.1103/PhysRevLett.93.177401, 177401-1-4.

[41] Y. Tian, H. Jiang, P. Laiho, E.I. Kauppinen, Validity of measuring metallic and semiconducting single-walled carbon nanotube fractions by quantitative Raman spectroscopy, Anal. Chem. 90 (2018) 2517–2525, https://doi.org/10.1021/acs.analchem.7b03712.

[42] A.A. Polokhin, YuO. Fedorova, A. Yu Gerasimenko, Vibrational spectroscopy of tissue-engineered structures based on proteins, chitosan, and carbon nanotube conjugates, Proc. SPIE Biophotonics 10685 (2018), https://doi.org/10.1117/12.2306639, 106853H-1.

[43] I.I. Bobrinetsky, A.Yu Gerasimenko, V.M. Podgaetsky, M.S. Saveliev, Spectral characteristics of materials based on carbon nanotubes, Biomed. Eng. 48 (2015) 30–34, https://doi.org/10.1007/s10527-015-9478-x.

[44] A.Yu Gerasimenko, L.P. Ichkitidze, U.E. Kurilova, D.T. Murashko, D.A. Potapov, Hardness maps analysis of the layered nanocomposites for tissue repair of the cardiovascular system, AIP Conference Proceedings 2140 (2019), 020022, https://doi.org/10.1063/1.5121947.

[45] C. Changlun, L. Bo, O. Akihisa, W. Xiangke, N. Masaaki, Oxygen functionalization of multiwall carbon nanotubes by microwave-excited surface-wave plasma treatment, J. Phys. Chem. 113 (2009) 7659–7665, https://doi.org/10.1021/jp9012015.
[46] Z. Luo, A. Oki, L. Carson, L. Adams, G. Neelgund, N. Soboyejo, G. Regisford, M. Stewart, K. Hibbert, G. Beharie, C. Kelly-Brown, P. Traisawatwong, Thermal stability of functionalized carbon nanotubes studied by in situ transmission electron microscopy, Chem. Phys. Lett. 513 (2011) 88–93, https://doi.org/10.1016/j.cplett.2011.07.072.
[47] A. Torres, L. Hoyos, J. Bustamante, A. Garay-Tapia, Direct functionalization of carbon nanotubes with phosphate, J. Comput. Theor. Nanosci. 13 (2016) 7640–7648, https://doi.org/10.1166/jctn.2016.5765.
[48] V.C. Lin, J.L. Koenig, Raman studies of bovine serum albumin, Biopolimers 15 (1976) 203–218, https://doi.org/10.1002/bip.1976.360150114.
[49] M.C. Chen, R.C. Lord, Laser-excited Raman spectroscopy of biomolecules. VIII. Conformational study of bovine serum albumin, J. Am. Chem. Soc. 98 (1976) 990–992, https://doi.org/10.1021/ja00420a021.
[50] N.–T. Yu, Comparison of protein structure in crystals, in lyophilized state, and in solution by laser Raman scattering. III. .alpha.-Lactalbumin, J. Am. Chem. Soc. 96 (1974) 4664–4668, https://doi.org/10.1021/ja00821a049.
[51] A.M. Bellocq, R.C. Lord, R. Mendelsohn, Laser-excited Raman spectroscopy of biomolecules. III. Native bovine serum albumin and β-lactoglobulin, Biochim. Biophys. Acta 257 (1972) 280–287, https://doi.org/10.1016/0005-2795(72)90280-2.
[52] P.C. Painter, J.L. Koenig, Raman spectroscopic study of the proteins of egg white, Biopolymers 15 (1976) 2155–2166, https://doi.org/10.1002/bip.1976.360151105.
[53] K. Nakamura, S. Era, Y. Ozaki, M. Sogami, T. Hayashi, M. Murakami, Conformational changes in seventeen cystine disulfide bridges of bovine serum albumin proved by Raman spectroscopy, PERS Letters 417 (1997) 375–378, https://doi.org/10.1016/S0014-5793(97)01326-4.
[54] G.N. Ten, A.Y. Gerasimenko, N.E. Shcherbakova, V.I. Baranov, Interpretation of IR and Raman Spectra of Albumin vol. 19, Izvestiya of Saratov University. New series. Series Physics, 2019, pp. 43–57.
[55] G.N. Ten, O.E. Glukhova, M.M. Slepchenkov, I.I. Bobrinetskii, R.A. Ibragimov, G.E. Fedorov, V.I. Baranov, Influence of topological defects on the structure of G and D spectral bands of a single-layer carbon nanotube, Opt Spectrosc. 120 (2016) 732–739, https://doi.org/10.1134/S0030400X16050258.